

Investigation of Aeroelastic Effects for a Helicopter Main Rotor in Hover

Manfred Imiela
German Aerospace Center
Institute of Aerodynamics and Flow Technology
Lilienthalplatz 7, 38108 Braunschweig, Germany
manfred.imiela@dlr.de

Abstract

In the search of new rotorblades with increased performance and reduced noise emissions blade shapes become more and more complex. Due to this phenomenon and the slender form of the blades themselves Fluid-Structure-Interaction (FSI) becomes increasingly important. Therefore an optimization framework with a loose coupling approach in the loop between the block-structured 3D Navier-Stokes solver FLOWer and the Comprehensive Rotor Code HOST has been developed. In order to assess the influence of the FSI optimizations are first conducted on a pure aerodynamic basis. In a second step the optimizations are repeated with the same parameter combinations using the full loose coupling procedure. The results are then compared in order to isolate the effects of FSI. Various parameter combinations are analyzed since FSI heavily depends on the planform and therefore on the chosen parameters.

1. Introduction

The design of helicopter rotor blades is a quite challenging task. While high fidelity computer analyses in the fixed wing community are widely employed today, the rotary wing community still relies heavily on low fidelity models. Although being less time consuming, the ability of these models to reproduce the behaviour of the physical model vanishes quickly with increasing complexity of the geometry. Since CFD has reached a sophisticated level of maturity, manufacturers are on the verge of integrating these methods into their design process. Because of the high aspect ratio of rotor blades FSI needs to be taken into account. This helps to reduce the number of design cycles. Most studies during the last 30 years such as [2] and [10] were devoted to aeroelastic and dynamic optimization with the aim of reducing vibratory loads and dynamic stresses. The majority of these works has relied on simple aerodynamic models based on blade element momentum theory because the application of

CFD inside the optimization was prohibitively expensive. In recent years some works such as [3], [4], [8], [9] have put their focus on the optimization of aerodynamic efficiency. While these studies have already incorporated CFD analysis tools within the optimization loop most works have mainly relied on pure aerodynamic computations. Therefore the uncertainty about the efficiency improvements of the new rotor blade persists.

The goal of this paper is to investigate the effects of FSI when integrated into the optimization process. Therefore two optimization schemes have been developed. In the first case the computations are carried out on a pure aerodynamic basis regarding the blade as rigid. The CFD analysis is realized with the block-structured 3D Navier-Stokes solver FLOWer. Steady computations on periodic meshes are used in order to reach short turnaround times. In the second case a loose Fluid-Structure-Coupling approach between FLOWer and the Comprehensive Rotorcode HOST from Eurocopter is applied in order to account for the blade dynamics and elasticity. The structural model consists of an extended 1D Euler-Bernoulli beam model. In the first step the motion and the deformations of the blade are transferred to the flow solver. Subsequently the loads and geometric changes of the blade planform are communicated to the structural model. The properties of the structural model themselves are not modified during the optimization.

The optimization is focused on improving the aerodynamic performance. The EGO method has been chosen as optimization algorithm since its effectiveness has been verified in [6]. First the general strategy of the optimization procedure is introduced. Secondly the parameterization and the grid generation are described. For detailed information on the solvers, the weak coupling procedure and optimization algorithms see [6]. The optimizations are first carried out with few design variables since their individual effect should be analyzed. An optimization with all design variables is conducted to demonstrate the full capacity of the framework.

2. Optimization Framework

The optimization framework as shown in Figure 1 consists of three elements, i.e. the optimizer, the preprocessing module and the fluid-structure module. The DAKOTA-Software from Sandia Labs [1] is used as optimization tool. It contains different optimization algorithms and steers the overall process by generating the design parameter sets, starting the individual evaluations and collecting the result from each analysis. The parameter set is then passed to the preprocessing unit where the mesh is created. The preprocessor starts with a series of 2D profiles which are lined up on the quarter chord line along the blade radius. The resulting 3D blade surface is then transferred to the grid generator where the volume mesh of the computational domain is generated. In a last step the monoblock grid is partitioned into multiple blocks in order to make it applicable to a parallel computation.

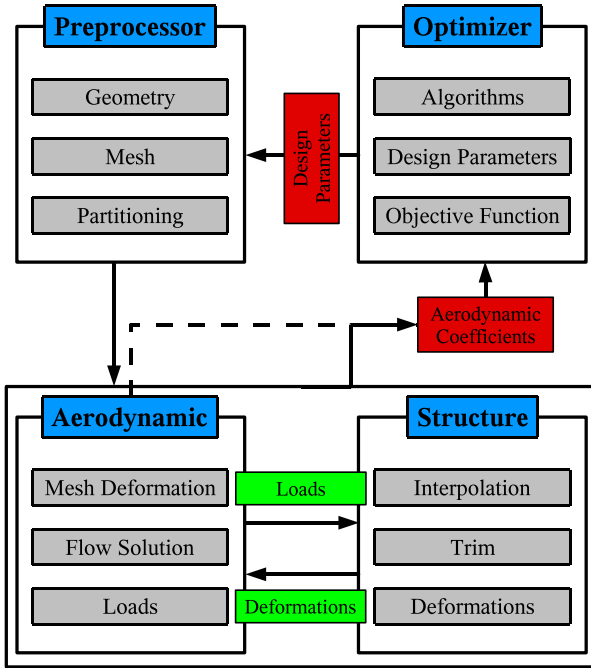


Figure 1: Flowchart of the optimization framework

The fluid-structure module is initiated by a trim computation with HOST. This delivers the dynamic response of the rotor and the elastic deformation which serve as input for the flow computation. After the periodic coupling has been carried out for a predefined number of iterations, the aerodynamic coefficients are extracted and passed to the optimizer which decides upon the next set of design parameters. The process is continued until the improvement falls below a predefined threshold.

2.1. Design Variables

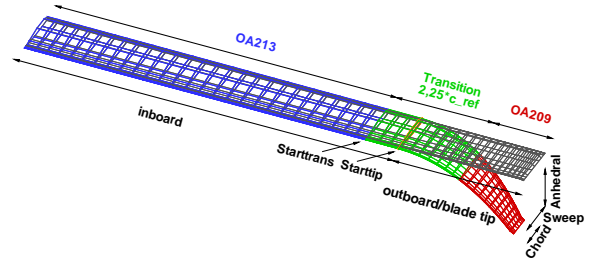


Figure 2: Design Parameters of the optimization process

The amount of evaluations during an optimization depends on the number of design variables. Because CFD computations are very time consuming, it is important to limit the number of design parameters. A trade off between the possibility of designing complex planforms and the number of design variables has to be made. Figure 2 shows the design variables, i.e. Twist, Sweep, Taper, Anhedral, Starttrans (Starting point of transition to second profile), Starttip (Starting point of blade tip area). The parameters can be optimized separately or simultaneously. Changing the starting point of the blade tip will naturally only affect the design if at least one other parameter is chosen. The thickness of the blade can be controlled by varying the radial position of the transition between the two different airfoils. The twist is modified by changing the geometric twist over the blade span. While the geometric twist varies non-linearly over the blade span because of the two different profiles involved, it is ensured that the aerodynamic twist varies linearly. In order to avoid solidity effects the thrust weighted area is held constant. This means reducing the blade tip chord will result in an increased chord for the inboard part of the blade. Sweeping the blade is achieved by prescribing an inplane offset value for the quarter chord line at the outmost profile of the blade ($r/R = 1.0$). The sweep distribution is then given by a parabolic distribution law with zero deflection and zero slope at the starting point of the blade tip and the full deflection at the tip. The anhedral of the blade is realized in the same manner for the out of plane offset.

For optimizations in hover the collective pitch angle Θ_0 is also added as a design variable. This way the rotor thrust is not fixed during the optimization. Considering two rectangular blades, the one with the higher Collective will have the higher Figure of Merit as long as the flow is attached. Therefore the optimizer will strive towards high collective pitch angles assuring that the optimizer will reach the maximum Figure of Merit for each design configuration.

2.2. Grid Generation

Once the blade surface has been constructed according to the new design variables the algebraic grid generator GEROS [5] is used for meshing the computational domain. All grids show a C-H topology. The tab is modelled with a sharp trailing edge. The profile at the tip is degenerated to a single line. Optimizations are carried out on coarse meshes. In order to confirm the results the optimal rotor configuration at the end of each optimization run is being recomputed on the fine mesh. While $y+$ -values on the coarse meshes range between 3-4, for the fine meshes they lie below 1. Since GEROS is only capable of constructing monoblock meshes, grids have to be split afterwards in order to run the CFD computations in parallel.

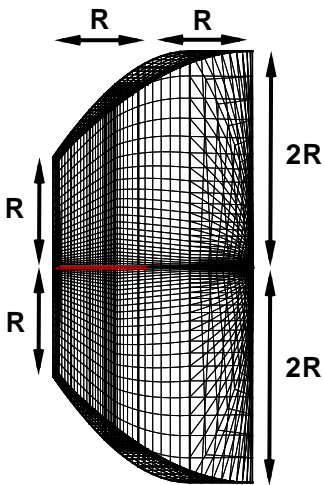


Figure 3: Dimensions of the computational domain

In hover the radial symmetry can be used to further reduce the computational domain as can be seen in Figure 3. Therefore only $\frac{1}{n}$ (n being the number of blades) of the domain has to be meshed. In order to assess the applicability of the coarse and fine mesh a mesh convergence study has been conducted. Table 1 contains the discretization of the different meshes that have been used. The bold numbers indicate the mesh discretization used for the optimization and verification.

Mesh	Elements (fine)	Elements (coarse)
1	256 × 84 × 64	128 × 42 × 32
2	208 × 80 × 64	104 × 40 × 32
3	176 × 72 × 64	88 × 36 × 32
4	152 × 48 × 48	76 × 24 × 24

Table 1: Mesh discretizations used for mesh convergence study: number of elements in chordwise × radial × normal direction

3. Optimization without FSC

3.1. Twist

Parameter	Initial	Final	Bounds
Collective[°]	10,0	26,69	4,0/30,0
Twist[°]	-4,32	-20,0	-20,0/0,0
Chord[*C _{ref}]	1,0	1,0	-
Sweep[*C _{ref}]	0,0	0,0	-
Anhedral[*C _{ref}]	0,0	0,0	-
Starttip[r/R]	0,806	0,806	-
Starttrans[r/R]	0,75	0,75	-
FM[-]	0,5135	0,6973	-

Table 2: Initial, final and bounded values for twist optimization without Fluid-Structure-Coupling

Table 2 shows the initial, final and bounded values of the twist optimization without Fluid-Structure-Coupling (FSC). On the basis of BEMT Leishman derives in [7] a hyperbolic distribution as the optimal twist law. Therefore a linear aerodynamic twist law has been chosen because it is close to the hyperbolic distribution. In order to assure a good mesh quality the Twist has been bounded to a maximum of -20° . The 7A rotor serves as the baseline rotor for the optimization.

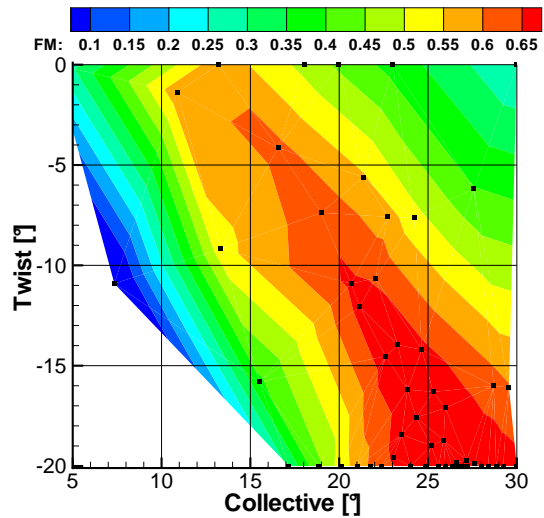


Figure 4: Figure of Merit as a function of the Twist and the Collective with rigid blades

Figure 4 shows the Figure of Merit as a function of the design variables. The black squares resemble parameter sets at which an evaluation with the flow solver has taken place. The color coding indicates the optimum at a high Collective in combination with a high Twist as has been expected.

The twist of the blade helps to reduce the induced power component. This is achieved through a triangular thrust distribution as can be seen in figure 5 thus resulting in a more uniform distribution of the induced velocity field. At the

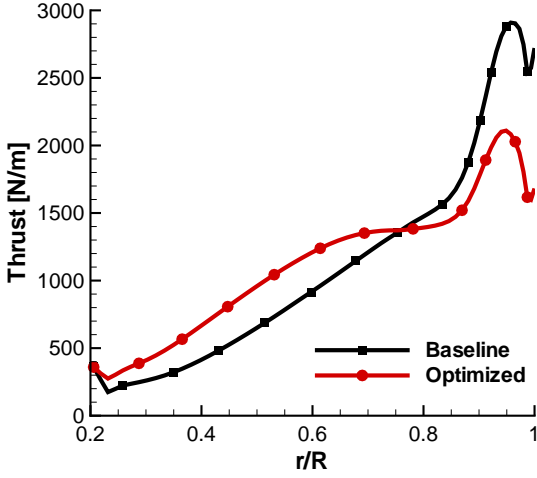


Figure 5: Radial thrust distribution of the baseline and optimized rotor with rigid blades on the fine mesh

blade tip where high tangential velocities are encountered due to the rotation of the blade the angle of attack is reduced by the twist, therefore decreasing the local thrust and consequently the local induced velocities. Inboard the local thrust and therefore the induced velocities are increased due to higher angles of attack. By reducing the thrust at the blade tip the blade tip vortex is also weakened which furthermore results in a decrease of the induced power.

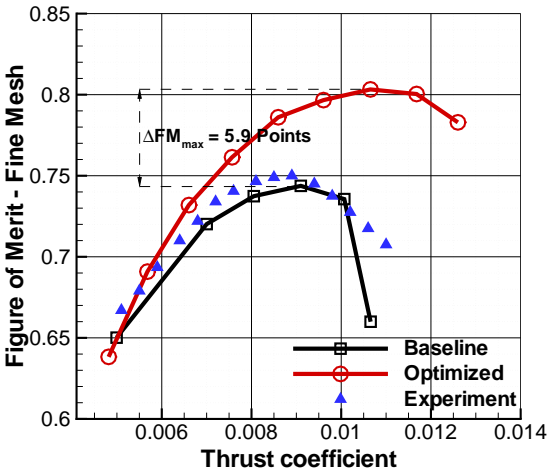


Figure 6: Polar of the baseline and twist optimized rotor with rigid blades on the fine mesh

In order to verify the result polars of the baseline and

the optimized rotor have been computed and are displayed in figure 6. The improvement of the optimized rotor can clearly be seen and extends over the whole range of thrust coefficients. The maximum gain of the optimized rotor adds up to six points and can be found at a higher thrust coefficient than for the baseline rotor as was expected. The comparison of the baseline and the experimental values exhibit small discrepancies for low thrust coefficients which are due to the missing of the blade cuff in the numerical analysis and the fully turbulent simulation. The rapid decrease of the Figure of Merit for the baseline rotor at high thrust coefficients can be accounted to a flow separation which starts to occur at the blade tip. In contrary this phenomenon is not observed in the experiment because the FSI will naturally be accounted for.

3.2. Sweep

Parameter	Initial	Final	Bounds
Collective[°]	10,0	16,27	4,0/30,0
Twist[°]	-4,32	-4,32	-
Chord[*C _{ref}]	1,0	1,0	-
Sweep[*C _{ref}]	0,0	-1,0	-1,0/1,0
Anhedral[*C _{ref}]	0,0	0,0	-
Starttip[r/R]	0,806	0,806	-
Starttrans[r/R]	0,917	0,917	-
FM[-]	0,4998	0,65779	-

Table 3: Initial, final and bounded values for Sweep optimization without Fluid-Structure-Coupling

Table 3 shows the initial, final and bounded values of the Sweep optimization without FSC. The Sweep describes the horizontal offset of the quarter-chord line as a multiple of chords at the blade tip. A parabolic distribution between the blade and the blade tip assures a smooth design. The bounds have been set to ± 1 which results in a maximum sweep angle of $\pm 33.2^\circ$ in order to avoid unrealistically high values. A modified version of the 7A rotor (different transition point between profiles) has been chosen as the baseline rotor.

Figure 7 depicts the Figure of Merit as a function of the design variables. The optimum can be found for a moderate Collective and maximum forward Sweep. The improvement is quite small though, since the rotational speed in hover is not high enough to create a shock. Therefore the enhancement is not caused by a reduction of the wave drag but a modification of the radial thrust distribution as is suggested by figure 8. Although the effect of Sweep on the thrust distribution is marginal, figure 8 shows that forward Sweep leads to an unloading of the blade tip while backward Sweep increases the blade tip loading.

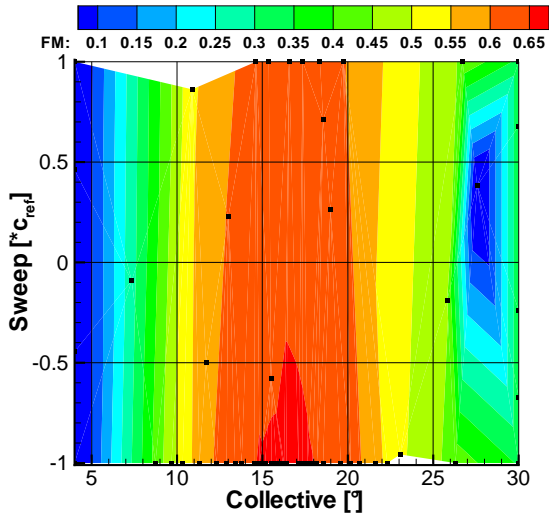


Figure 7: Figure of Merit as a function of the Sweep and the Collective with rigid blades

The improvement is indeed valid for a wide range of thrust coefficients as can be seen in figure 9. While the polar on the coarse mesh reveals a flat plateau at the maximum Figure of Merit, it drastically decreases on the fine mesh at high thrust coefficients as can be seen in figure 10.

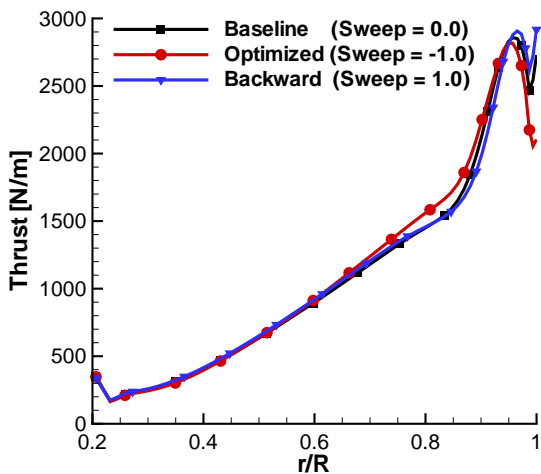


Figure 8: Radial thrust distribution of the baseline, optimized and maximal backwards swept rotor with rigid blades on the fine mesh

The reason for this behaviour can be observed in figure 11. While the flow is still attached on the coarse mesh, a strong vortex has formed on the fine mesh at the blade tip which results in a detachment of the flow. This causes a strong decrease in thrust and an increase in power leading

to a strong decay of the Figure of Merit.

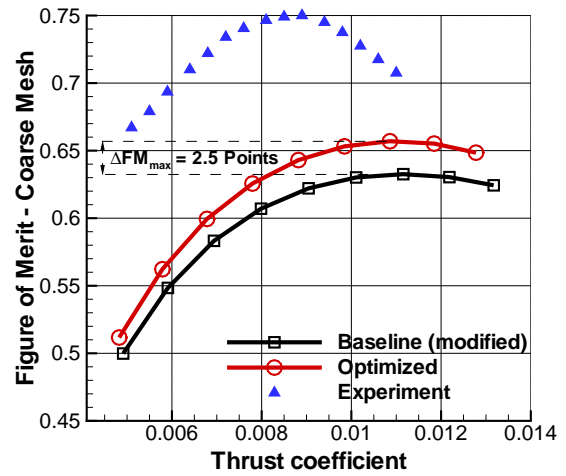


Figure 9: Polars of baseline and optimally swept rotor with rigid blades on the coarse mesh

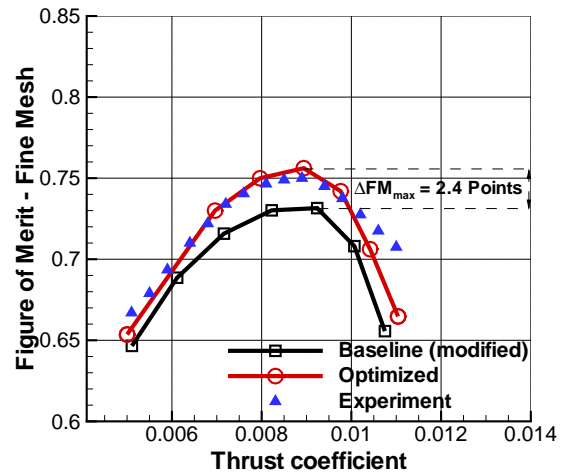
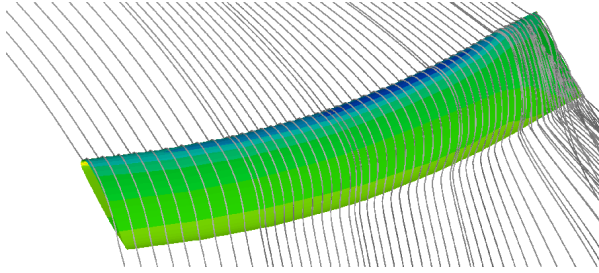
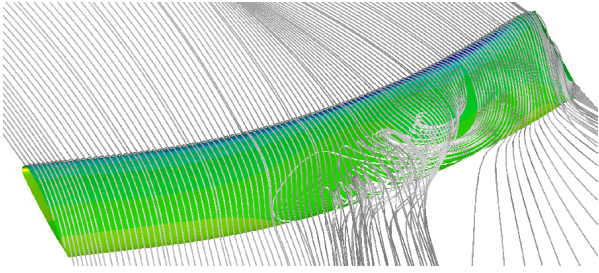


Figure 10: Polars of baseline and optimally swept rotor with rigid blades on the fine mesh

The example indicates that care has to be taken when optimizing on coarse meshes. While the efficiency and reliability of the process could be demonstrated in the first case, this example shows that the procedure is limited. Flow detachments occur in highly loaded areas which in this case is the blade tip due to high flow velocities and angles of attack. The inclusion of the Twist alleviates this by reducing the angle of attack at the blade tip. Therefore this example underlines the importance of the choice of the design parameters.



(a) Attached flow on coarse mesh



(b) Detached flow on fine mesh

Figure 11: Flow visualization of the optimally swept rotor with rigid blades on coarse and fine mesh

3.3. All Parameters

Parameter	Initial	Final	Bounds
Collective[°]	10,0	25,34	4,0/30,0
Twist[°]	-4,32	-17,49	-20,0/0,0
Chord[*c _{ref}]	1,0	0,5	0,5/1,5
Sweep[*c _{ref}]	0,0	-1,0	-1,0/1,0
Anhedral[*c _{ref}]	0,0	-0,33	-1,0/1,0
Starttip[r/R]	0,806	0,761	0,415/0,962
Starttrans[r/R]	0,75	0,916	0,415/0,917
FM[-]	0,5135	0,71201	-

Table 4: Initial, final and bounded values for optimization with all parameters without Fluid-Structure-Coupling

Table 4 shows the initial, final and bounded values of the optimization of all parameters without FSC. The test case has been chosen in order to extend the parameter space as much as possible. As before the Twist has been limited to -20° for reasons of mesh quality. Sweep and Anhedral are bounded to a value of ± 1 since higher values will cause problems when FSC comes into play. The Chord has been restricted to half the reference chord since lower values will cause problems for the manufacturing. The starting of the blade tip and the transition point of the airfoils have been allowed to the most outboard possible section to guarantee a parameter space as big as possible, yet allowing for the other design parameters to take effect.

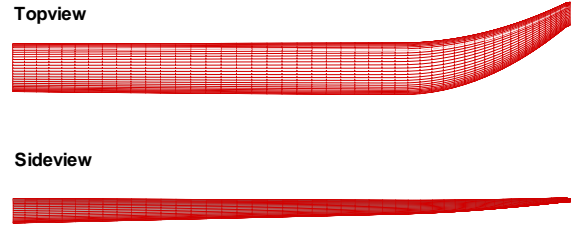


Figure 12: Optimization of all parameters with rigid blades: Topview and sideview of the forward swept rotor

Figure 12 presents the top- and sideview of the optimized blade. Opposed to the previous optimization the Twist ensures an unloading of the tip. The combination of Twist and Sweep leads to a dihedral which is compensated by the Anhedral given by the design parameter.

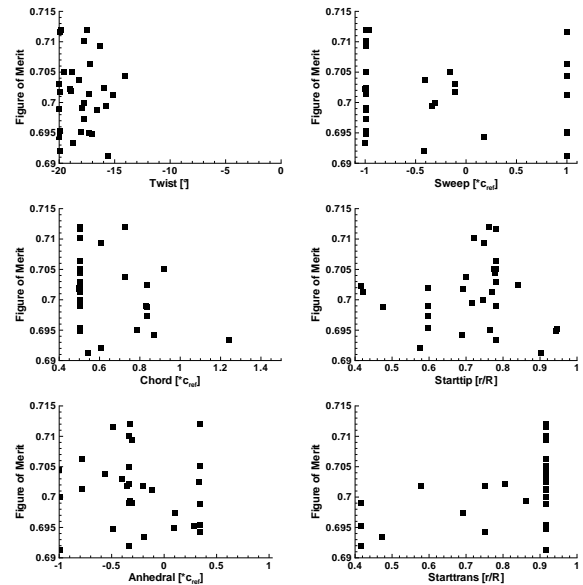


Figure 13: Optimization of all parameters with rigid blades: Figure of Merit as a function of the design parameters

Figure 13 depicts the correlation between the goal function and the design parameters. The Collective yields an optimal value of about 25° . A quite high Twist of -17° helps to balance the thrust distribution in the right way as can be seen in figure 14. A comparison with the thrust loading of the Twist optimization (figure 5) shows that the decrease of the chord at the blade tip leads to a further unloading of the blade tip.

The modification of the profile transition points act in the same manner. The thicker OA213 profile extends over

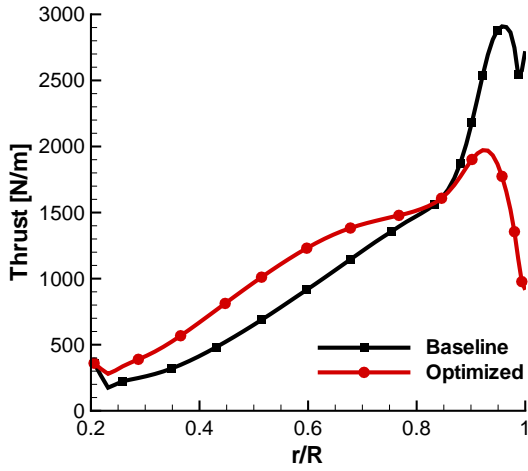


Figure 14: Radial thrust distribution of the baseline and optimized rotor with rigid blades on the fine mesh

a wider range and therefore produces more thrust between 75% and 90% radius. Moreover the change of the profile transition leads to an increase of twist since the difference of the different zero incidence angles is not fully taken into account as can be seen in figure 15.

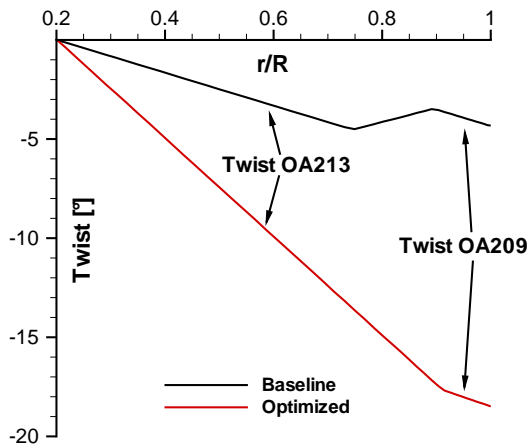


Figure 15: Geometric twist of the baseline and optimized rotor with rigid blades

The design parameters Twist, Chord, Starttip and Starttrans exhibit a clear relationship, while Sweep and Anhedral show an ambiguous behaviour. Besides the optimal value for the Anhedral which is given in the table, figure 13 suggests that other solutions between -0.5 and $+0.35$ could also have been chosen. For the Sweep the variety of solutions even varies between ± 1 which are the left and right bounds for the design parameter. In fact those two design parameters

only have a minor effect on the goal function and therefore the final values heavily depend on the outcome of the other parameters.

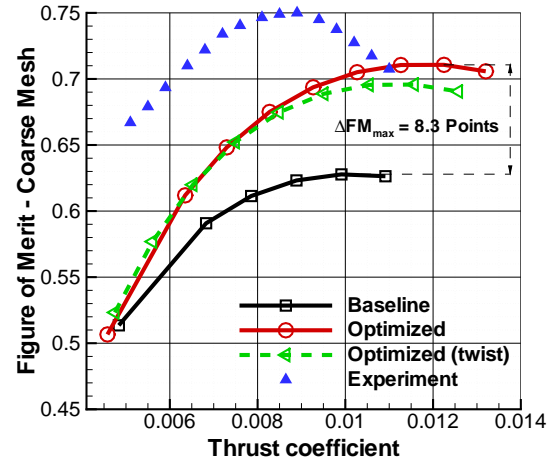


Figure 16: Optimization of all parameters with rigid blades: Polar of the baseline and optimized rotor on the coarse mesh

Figure 16 shows the polar of the baseline and optimized rotor on the coarse mesh. In comparison to the Twist optimization the Figure of Merit could additionally be raised by 1 point. The improvement though is limited to the coarse mesh. On the fine mesh both rotors reach approximately the same maximum Figure of Merit. The optimized rotor (all parameters) even shows the disadvantage of having a worse stall behaviour at high thrust coefficients compared with the Twist optimized rotor which is again due to the distinct forward Sweep as in the previous example.

4. Optimization including FSC

4.1. Twist

Parameter	Initial	Final	Bounds
Collective[°]	10,0	28,16	4,0/30,0
Twist[°]	-4,32	-20,0	-20,0/0,0
Chord[*C _{ref}]	1,0	1,0	-
Sweep[*C _{ref}]	0,0	0,0	-
Anhedral[*C _{ref}]	0,0	0,0	-
Starttip[r/R]	0,806	0,806	-
Starttrans[r/R]	0,75	0,75	-
FM[-]	0,4913	0,6962	-

Table 5: Initial, final and bounded values for twist optimization including FSC

Table 5 shows the initial, final and bounded values of the twist optimization with FSC. As in the previous case a linear aerodynamic twist law has been chosen. Also the boundary condition, the baseline rotor, etc. have stayed unmodified except the computational approach has been changed from a pure aerodynamic analysis to an aeroelastic modelling using the loose coupling strategy between FLOWer and HOST as has been described before.

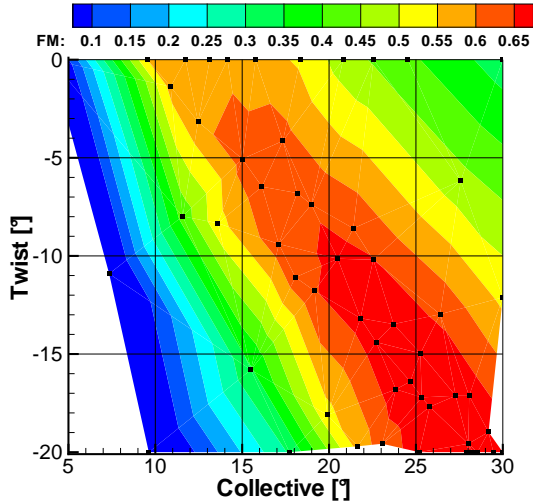


Figure 17: Figure of Merit as a function of the Twist and the Collective with elastic blades

As can be seen from figure 17 FSI has an effect on the shape of the goal function. Compared to the rigid optimization case the goal function exhibits a much wider optimal region. Nevertheless the consideration of FSI does not have an influence on the outcome of the optimization. Table 5

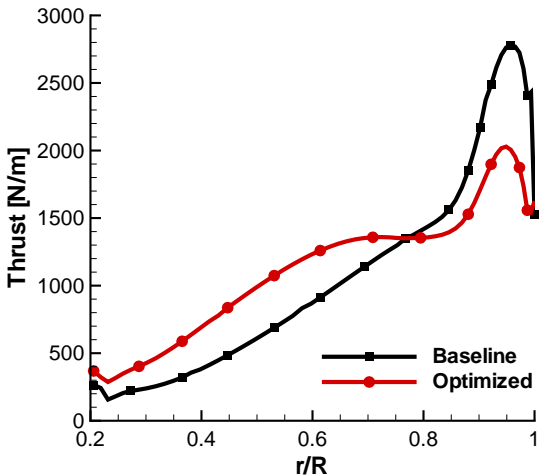


Figure 18: Radial thrust distribution of the baseline and optimally twisted rotor with elastic blades on the fine mesh

clearly shows that the optimization result with FSI is almost the same than without it. Merely the final value for the Collective is slightly higher than without FSI. The reason for this is that the elastic torsion acts in the same way as the Twist of the blade, i.e. it changes the local angle of attack in order to achieve a more uniform induced velocity field. This has already been very well attained in the rigid case and therefore no additional improvement can be made.

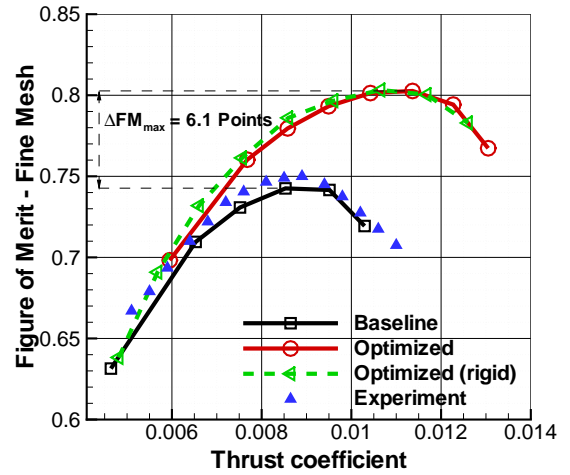


Figure 19: Polar of the baseline and optimally twisted rotor with elastic blades on the fine mesh

Effectively the elastic torsion provides for a good-natured stall behaviour. That is the reason for a smoother decrease of the Figure of Merit of the baseline rotor at higher thrust coefficients as can be seen in figure 19. The comparison of the polars with and without FSI show only very small differences as the optimization itself.

4.2. Sweep

Parameter	Initial	Final	Bounds
Collective[°]	10,0	30,00	4,0/30,0
Twist[°]	-4,32	-4,32	-
Chord[*C _{ref}]	1,0	1,0	-
Sweep[*C _{ref}]	0,0	0,34	-1,0/1,0
Anhedral[*C _{ref}]	0,0	0,0	-
Starttip[r/R]	0,806	0,806	-
Starttrans[r/R]	0,917	0,917	-
FM[-]	0,447	0,6872	-

Table 6: Initial, final and bounded values for sweep optimization including FSC

The layout of the optimization is identical to the first Sweep optimization except for the FSC. Table 6 shows the

initial, final and bounded values of the Sweep optimization including FSC. As can be seen the FSC leads to a drastically different result than without FSC. While in the pure aerodynamic case a maximum forward Sweep proved to be optimal, a moderate backward Sweep shows to be superior in the FSC case. Moreover a forward Sweep value greater

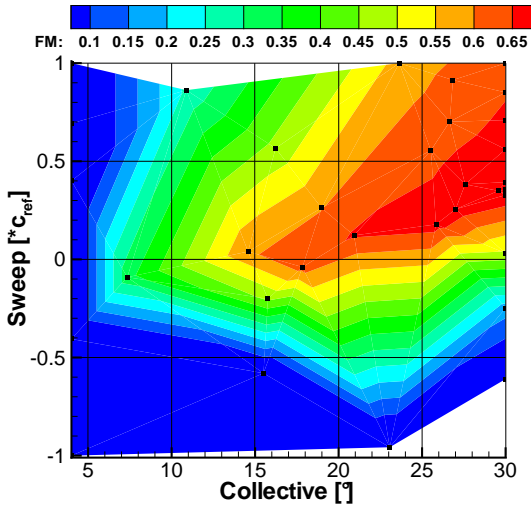


Figure 20: Figure of Merit as a function of the Sweep and the Collective with elastic blades

than 0.5 will return a quite poor value for the Figure of Merit as is presented in figure 20. This is due to the instable nature of forward swept rotors. As can be seen the shape of the goal function also considerably varies from the goal function without FSC.

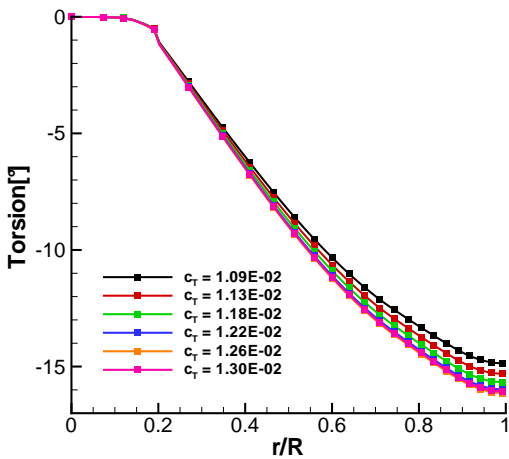


Figure 21: Elastic Torsion of optimally swept rotor with elastic blades at various thrust coefficients on fine mesh

The reason for this can be found regarding the elastic torsion in figure 21. Due to the swept blade tip the aero-

dynamic forces do not act at the quarter-chord-line but at an excentric point causing the blade to twist. This way the elastic torsion takes over the part of the Twist and helps to unload the tip allowing for a much higher Collective and therefore a higher Figure of Merit.

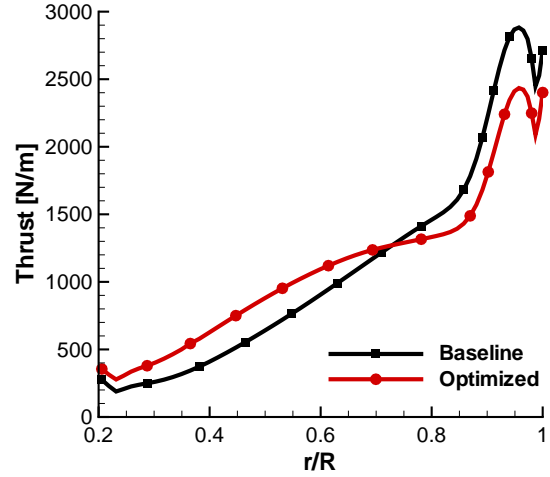


Figure 22: Radial thrust distribution of the baseline and optimally swept rotor with elastic blades on the fine mesh

The improvement for the Figure of Merit is not only limited to a single optimization point but can be observed for all thrust coefficients as depicted in figure 23. The result from

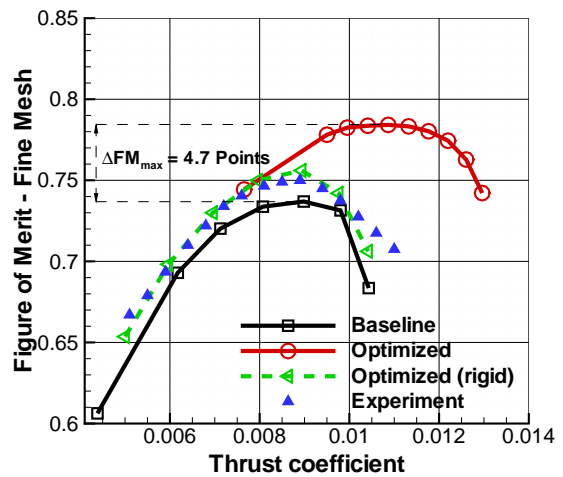


Figure 23: Polars of baseline and optimally swept rotor with elastic blades on fine mesh

the sweep optimization with rigid blades is marked for comparison (triangles, dashed line). Furthermore the optimized rotor provides for a wide plateau at the maximum Figure of Merit and a gradual decrease after the maximum point has been surpassed. As in previous cases the design modi-

fications result in a better thrust distribution over the blade radius as shown in Figure 22. While the loading at the blade tip is decreased, the loading is raised inboard thus giving a more uniform distribution of the induced velocities.

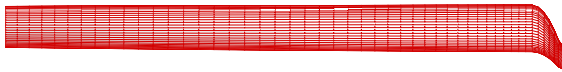
4.3. All Parameters

Parameter	Initial	Final	Bounds
Collective[°]	10,0	29,98	4,0/30,0
Twist[°]	-4,32	-19,95	-20,0/0,0
Chord[*c _{ref}]	1,0	0,5	0,5/1,5
Sweep[*c _{ref}]	0,0	0,87	-1,0/1,0
Anhedral[*c _{ref}]	0,0	0,008	-1,0/1,0
Starttip[r/R]	0,806	0,961	0,415/0,962
Starttrans[r/R]	0,75	0,561	0,415/0,917
FM[-]	0,4913	0,70537	-

Table 7: Initial, final and bounded values for optimization with all parameters including Fluid-Structure-Coupling

The previous example shows that the effect of the FSC greatly depends upon the choice of the parameters. While the twist optimization is not affected by the FSC, blade Sweep dramatically changes the aeroelastic behaviour. For the optimization of all parameters with consideration of FSC a distinctive influence is evident. Compared to the previous optimization with all parameters, the boundary conditions, baseline rotor, optimizer, etc. have not been altered except the solver has changed from pure aerodynamic to a loose coupling approach. Table 7 shows the initial, final

Topview



Sideview



Figure 24: Optimization of all parameters with elastic blades: Top- and sideview of the backward swept rotor

and bounded values of the optimization of all parameters including FSC. Compared to the case without FSC only the value for the Chord is identical. The final Collective and Twist values end up being higher. While the optimization without FSC returns a forward swept blade, in the case with FSC the blade turns out to have a strong backward Sweep as can be seen in figure 24. The reason for this has already been described in section 3.2. The varied starting point of

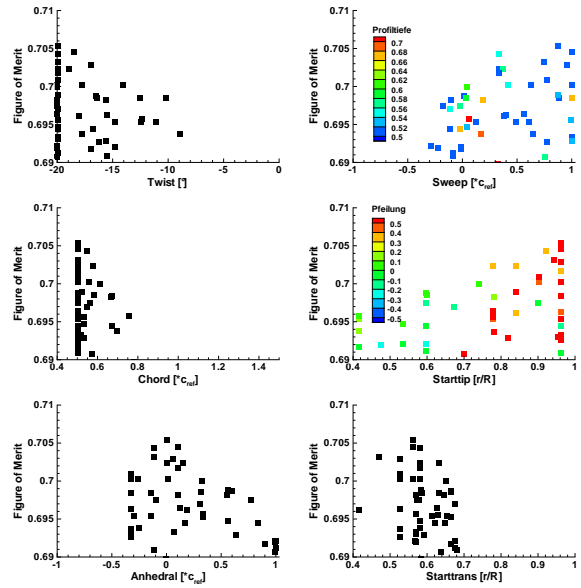


Figure 25: Optimization of all parameters with elastic blades: FM as a function of the design parameters

the blade tip marks another major difference. Without FSC the initiation point is located at 76% radius resulting in a big blade tip while this point is moved outboard as far as possible in the case of FSC. This is due to the fact that the elastic torsion will increase as the blade tip becomes bigger finally reaching its structural limits. The distribution of the two baseline profiles OA213 and OA209 also differs. With FSC the thinner profile extends over a bigger portion of the blade radius resulting in less thrust in this region which leads to an additional unloading of the blade tip.

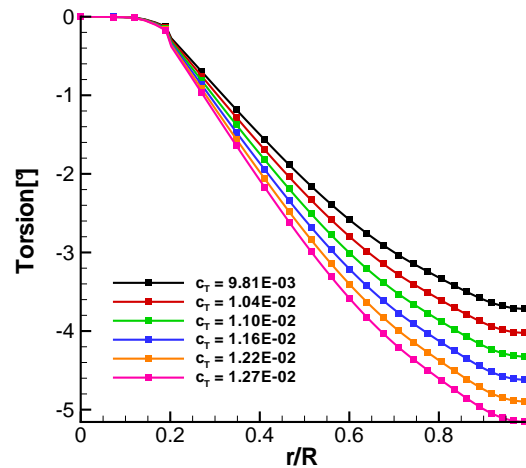


Figure 26: Elastic Torsion of optimized rotor with elastic blades at various thrust coefficients on fine mesh

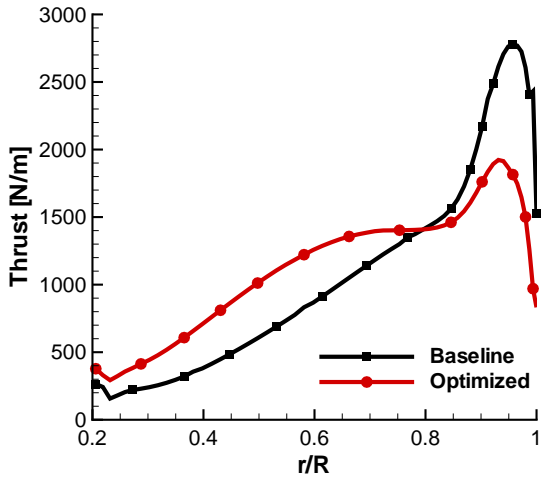


Figure 27: Radial thrust distribution of the baseline and optimized rotor with elastic blades on the fine mesh

Figure 25 shows the relationship between the design parameters and the Figure of Merit. As can be seen the design parameters nicely correlate with the goal function opposed to the case without FSC. With FSC a unique optimum can clearly be defined by simply following the trend of the optimization results. The color coding for the Sweep additionally indicates that designs with a high Sweep value feature a small Chord value. The small tip Chord is favoured in combination with high Sweep because it ensures that the elastic torsion which is shown in figure 26 does not become too big due to a smaller blade tip area. The color coding for the Starttip emphasizes that the further outboard the starting point of the blade tip the higher the Sweep. The reasons for that have been explained above.

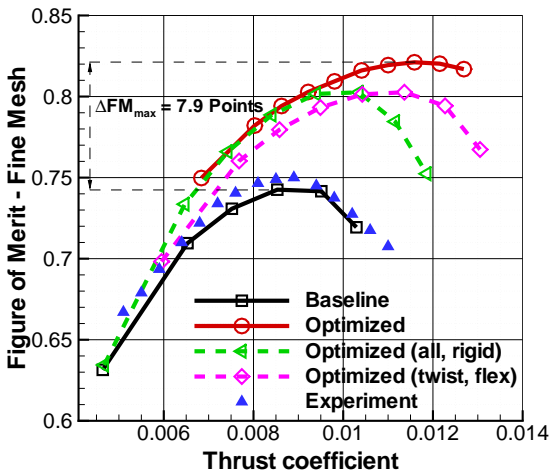


Figure 28: Optimization of all parameters with elastic blades: Polar of the baseline and optimized rotor on the fine mesh

Figure 27 presents the radial thrust distribution of the optimized blade. Clearly the optimization with all parameters including FSC provides the highest unloading of the blade tip and the best radial thrust distribution. Consequently the optimization yields the highest improvement for the Figure of Merit as is displayed in figure 28. For comparison not only the polars of the baseline and the optimized rotor are plotted but also the polars of the optimization with all parameters in the rigid blade case and the polar of the twist optimized blade with FSC.

4.4. Synopsis

The previous examples have made clear that FSC can play an important role. In order to summarize the results and to give an overview of the optimizations with different parameter combinations the maximum Figure of Merit of each optimization is presented for the rigid blade case in figure 29 and for the elastic blade case in figure 30. The

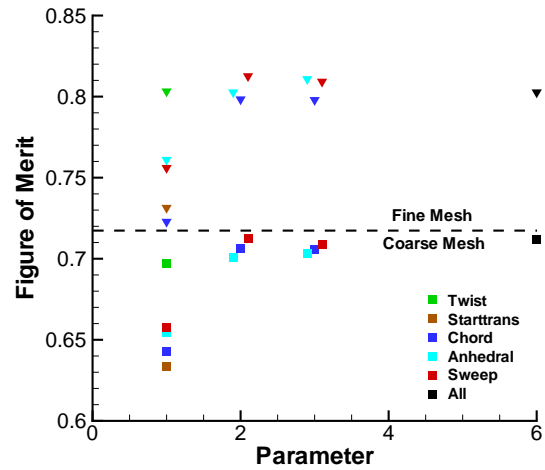


Figure 29: Optimizations without FSC with different parameter combinations: coarse and fine mesh

graphs are splitted into two parts - one for the optimizations (coarse mesh), and one for the verifications (fine mesh). The color coding indicates the different design parameters in the single parameter case; optimizations with two parameters additionally include the Twist beside the other design parameter (Chord, Sweep or Anhedral). Optimizations with three parameters include the Twist and Starttip besides the given parameter. Both figures show that Twist leads to the best result for the single parameter optimization. The other parameters attain much lower values. This is due to the fact that the Collective cannot be increased for those parameters as much as for the Twist because stall will occur at the blade tip due to the high angles of attack. One will also recognize that the result for Sweep is much lower in the rigid case than in the elastic case. This is due to the elastic torsion. In

both cases the optimization (coarse mesh) with all parameters yield the highest or almost highest goal function. In the rigid case unfortunately the results for the 2 parameter optimizations reach a higher Figure of Merit than for the 3 parameter optimization. The reason for this might be that the design parameters exhibit a different sensitivity and therefore interfere with each other. Fortunately this is not the case for the elastic blade. The ordering of the optimization cases is very well kept on the fine meshes which indicates that the procedure is working reliably. Only optimizations with Chord often perform worse on the fine meshes which will be due to the fact that a rotor with a small Chord will encounter stall on the fine but not on the coarse meshes.

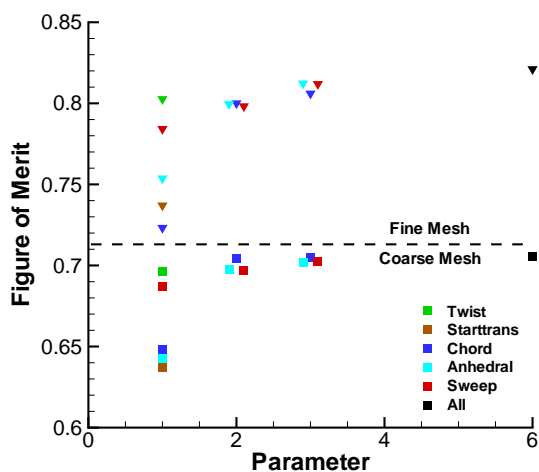


Figure 30: Optimizations including FSC with different parameter combinations: coarse and fine mesh

5. Conclusion

The influence of FSC has been investigated through automatic optimization with various parameters using CFD analyses and coupled CFD-CSM analyses within the optimization loop. The goal of the work was to extensively verify the framework and to analyse the principal effects of different design parameters. The following conclusions can be drawn from this study:

1. Optimizations in hover pursue the goal of reaching a triangular thrust distribution. Therefore the loading must be decreased at the blade tip and be shifted in-board.
2. Twist is the most sensitive parameter. It directly acts on the induced velocities.
3. Effect of Sweep, Chord and Anhedral on aerodynamics are small when optimized separately (only 2.order).

Therefore the parameter combination plays an important role. If Sweep is optimized, Twist needs to be optimized also.

4. Parameters should generally be optimized together. In general the optimization will produce better results the more design parameters are included given the fact that the optimization does not become stiff.
5. Optimization of Twist, Chord and Anhedral are independent of FSC.
6. Sweep shows strong FSI effects. The driver is the elastic torsion.
7. FSC leads to a more physical representation which can help avoid irritations of the optimization algorithm due to non-physical behaviour.

References

- [1] B. Adams. The dakota toolkit for parallel optimization and uncertainty analysis. In *SIAM Conference on Optimization*, Boston, MA, May 2008.
- [2] A. Chattopadhyay and Y. D. Chiu. An enhanced integrated aerodynamic load/dynamic optimization procedure for helicopter rotor blades. Contractor Report NASA CR-4326, National Aeronautics and Space Administration, Langley Research Center Hampton, VA 23665-5225, Oct 1990.
- [3] K. Collins, J. Bain, N. Rajmohan, L. Sankar, T. A. Egolf, R. D. Janakiram, K. Brentner, and L. Lopes. Toward a high-fidelity helicopter rotor redesign framework. In *American Helicopter Society 64th Annual Forum*, 2008.
- [4] A. Dumont, A. LePape, J. Peter, and S. Huberson. Aerodynamic shape optimization of hovering rotors using a discrete adjoint of the rans equations. In *American Helicopter Society 65th Annual Forum*, 2009.
- [5] M. H. L. Hounjet, C. Allen, L. Vigeveno, N. Trivellato, A. Pagano, A. D'Alascio, and N. Jobard. Outline and application of geros: a european grid generator for rotorcraft simulation methods. Technical report, NLR, 1998.
- [6] M. Imiela. High-fidelity optimization framework for helicopter rotors. In *35th European Rotorcraft Forum*, 2009.
- [7] J. G. Leishman. *Principles of Helicopter Aerodynamics*. Cambridge University Press, New york, 2nd edition, 2006.
- [8] A. LePape. Numerical aerodynamic optimization of helicopter rotors: Multi-objective optimization in hover and forward flight conditions. In *31st European Rotorcraft Forum*, September 2005.
- [9] J. L. Walsh, K. C. Young, F. J. Tarzanin, J. E. Hirsh, and D. K. Young. Optimization issues with complex rotorcraft comprehensive analysis. In *7th AIAA/USAF/NASA/ISSMO Symposium on Multidisciplinary Analysis and Optimization*, number AIAA 98-4889, September 1998.
- [10] K. Yuan and P. Friedmann. Aeroelasticity and structural optimization of composite helicopter rotor blades with swept tips. Contractor Report 4665, National Aeronautics and Space Administration, Langley Research Center, Hampton, Virginia, May 1995.